ADVANCED FUNCTIONAL MATERIALS

Supporting Information

for *Adv. Funct. Mater.,* DOI: 10.1002/adfm.202111446

Site-Specific Axial Oxygen Coordinated FeN_4 Active Sites for Highly Selective Electroreduction of Carbon Dioxide

Ting Zhang, Xu Han, Hong Liu, Martí Biset-Peiró, Jian Li,* Xuan Zhang, Pengyi Tang, Bo Yang, Lirong Zheng,* Joan Ramon Morante, and Jordi Arbiol**

Supporting Information

Site-Specific Axial Oxygen Coordinated FeN_4 Active Sites for Highly Selective Electroreduction of Carbon Dioxide

Ting Zhang,[1,2‡]* Xu Han,[1‡] Hong Liu,[3‡] Martí Biset-Peiró,[2] Jian Li,[4]* Xuan Zhang,[5] Pengyi Tang,[6] Bo Yang,[3] Lirong Zheng,[7]* Joan Ramon Morante,[2,8] and Jordi Arbiol[1,9]*

[1]Catalan Institute of Nanoscience and Nanotechnology (ICN2), CSIC and BIST, Campus UAB, Bellaterra, 08193, Barcelona, Catalonia, Spain

[2]Catalonia Institute for Energy Research (IREC), Jardins de les Dones de Negre 1, Sant Adrià del Besòs, 08930, Barcelona, Catalonia, Spain

[3]School of Physical Science and Technology, ShanghaiTech University, 393 Middle Huaxia Road, Shanghai, 201210, P. R. China

[4]Laboratory of Renewable Energy Science and Engineering, Institute of Mechanical Engineering, EPFL, Station 9, 1015 Lausanne, Switzerland

[5]Department of Materials Engineering, KU Leuven, Kasteelpark Arenberg, 44, B-3001 Leuven, Belgium

[6]State Key Laboratory of Information Functional Materials, 2020 X-Lab, Shanghai Institute of Microsystem and Information Technology, Chinese Academy of Sciences, Shanghai, China

[7]Beijing Synchrotron Radiation Facility, Institute of High Energy Physics, Chinese Academy of Sciences, Beijing 100049, China

[8]Department of Physics, Universitat de Barcelona, 08028, Barcelona, Catalonia, Spain

[9]ICREA, Pg. Lluís Companys 23, 08010 Barcelona, Catalonia, Spain

Correspondence: ting.zhang@icn2.cat

Correspondence: jian.li@epfl.ch

Correspondence: zhenglr@ihep.ac.cn

Correspondence: arbiol@icrea.cat

Materials and Methods

Materials:

If not specified, all chemical reagents were purchased from Sigma-Aldrich. Zinc nitrate hexahydrate ($Zn(NO_3)_2 \cdot 6H_2O$), 2-Aminoterphthalic acid, iron chloride hexahydrate ($FeCl_3 \cdot 6H_2O$), 2-methylimidazole (2-mim), N,N-dimethylformamide (DMF), ethanol and sodium bicarbonate ($NaHCO_3$) were all of analytical grade and used as received without further purification. Meanwhile, all solutions were prepared with Milli-Q water (DI-H_2O, Ricca Chemical, ASTM Type I). The Nafion (N-117 membrane, 0.18 mm thick) was purchased from Alfa Aesar and kept in 0.5 M NaOH solution. The carbon paper was also purchased from Alfa Aesar.

Characterization:

The X-ray diffraction patterns (XRD) were obtained through a Bruker D4 X-ray powder diffractometer using Cu Kα radiation (1.54184 Å). Field emission scanning electron microscopy (FESEM) images were collected on a FEI Magellan 400 L scanning electron microscope. The transmission electron microscopy (TEM) and high angle annular dark field scanning TEM (HAADF-STEM) images were obtained in a Tecnai F20 field emission gun microscope with a 0.19 nm point-to-point resolution at 200 kV equipped with an embedded Quantum Gatan Image Filter for EELS analyses. Images have been analyzed by means of Gatan Digital Micrograph software. Parts of HAADF-STEM images and elemental mapping (EDX) were obtained in a spherical aberration-corrected (AC) transmission electron microscope FEI Themis Z and

operated at 200 kV. X-ray photoelectron spectroscopy (XPS) was performed on a Phoibos 150 analyser (SPECS GmbH, Berlin, Germany) in ultra-high vacuum conditions (base pressure 4×10^{-10} mbar) with a monochromatic aluminum Kα X-ray source (1486.74 eV). Binding energies (BE) were determined using the C 1s peak at 284.5 eV as a charge reference. Raman spectra were obtained using Senterra.

XAFS Measurements:

The X-ray absorption find structure spectra (Fe K-edge) were collected at 1W1B station in Beijing Synchrotron Radiation Facility (BSRF). The storage rings of BSRF were operated at 2.5 GeV with an average current of 250 mA. Using Si (111) double-crystal monochromator, the data collection was carried out in transmission/fluorescence mode using ionization chamber. All spectra were collected in ambient conditions.

XAFS Analysis and Results:

The acquired EXAFS data were processed according to the standard procedures using the ATHENA module implemented in the IFEFFIT software packages. The k^3-weighted EXAFS spectra were obtained by subtracting the post-edge background from the overall absorption and then normalizing with respect to the edge-jump step. Subsequently, k^3-weighted $\chi(k)$ data of Fe K-edge were Fourier transformed to real (R) space using a hanning windows (dk=1.0 $Å^{-1}$) to separate the EXAFS contributions from different coordination shells. To obtain the quantitative structural parameters around central atoms, least-squares curve parameter fitting was performed using the ARTEMIS module of IFEFFIT software packages.[1-3]

Synthesis Methods:

Preparation of IRMOF-3

The fabrication process of IRMOF-3 is according to previous report with minor modification.[4] Typically, 932 mg of $Zn(NO_3)_2 \cdot 6H_2O$ was dissolved in 100 mL DMF under magnetic stirring at room temperature to form a homogeneous solution. Then, 181 mg of 2-aminoterphthalic acid were added into the above mixture under ultrasonic until the formation of clear solution. The obtained homogeneous solution was transferred into the Teflon-lined stainless-steel autoclave and reacted at 100 ºC for 24 h. After cooling to room temperature, the powder was collected by centrifugation, washed with ethanol and DMF several times to remove organic residual. The final products were then dried in vacuum at 65 ºC for 4 h.

Preparation of ZIF-8

The fabrication of ZIF-8 is similar to the published report.[5] Typically, 1.115 g of $Zn(NO_3)_2 \cdot 6H_2O$ was dissolved in 50 mL methanol under magnetic stirring at room temperature to form a homogeneous solution. Then, 50 mL methanolic solution containing 1.232 g of 2-mim were added into the above mixture under ultrasonic until the formation of clear solution. The obtained homogeneous solution reacted at room temperature for 24 h without stirring. Then, the white powder was collected by centrifugation, washed with methanol several times to remove organic residual. The final products were then dried in vacuum at 60 ºC for overnight.

Preparation of Fe-IRMOF-3 and Fe-ZIF-8

In this procedure, the 100 mg of IRMOF-3 powder was dispersed in 10 mL DMF under ultrasound for 10 min at room temperature. After forming a homogeneous solution, $FeCl_3 \cdot 6H_2O$ aqueous solution (10 mg/mL, 20 μL) was dropwise injected into the above solution under ultrasound for 5 min at room temperature. Next, the mixed solution was under magnetic stirring at room temperature for 3 h. After reacting, the powder was collected by centrifugation, washed with ethanol and DMF several times to remove organic residual and dried in vacuum at 65 ℃ for 6 h. Then, we obtained the Fe-IRMOF-3. Similarly, Fe-ZIF-8 was prepared by replacing IRMOF-3 with ZIF-8.

Preparation of Disperse Fe-N-C (denoted as O-Fe-N-C and Fe-N-C)

As-prepared Fe-IRMOF-3 (or Fe-ZIF-8, or IRMOF-3) powders were put at the porcelain boat. Subsequently, the samples were placed in a tube furnace and heated at 950 °C for 2 h with heating rate of 5 °C/min under an Ar atmosphere to yield disperse O-Fe-N-C (or Fe-N-C, or N-C).

Preparation of O-Fe-N-C-Acid

In order to remove the Fe nanoparticle in O-Fe-N-C, we treated the O-Fe-N-C sample using 1 M H_2SO_4 for 48 h. After acid process, the powder was collected by centrifugation, washed with DI-H_2O and dried in vacuum at 60 ℃ overnight. Then, we obtained the O-Fe-N-C-Acid.

Ink Preparation:

2 mg synthesized different samples and 50 μL 5 wt% Nafion solutions were dissolved in ethanol (1 mL) and ultrasonicated for 30 min to form evenly suspension for the further electrochemical experiments. To prepare the working electrode, 500 μL above as-prepared inks were dropped onto the two sides of the carbon paper electrode with 1×1 cm^2 and then dried at room temperature for a few minutes, giving a catalyst loading mass of ~1 mg/cm^2.

Electrochemical Measurement:

The electrocatalytic performance of different catalysts was measured at room temperature by using a gas-tight H-cell with two-compartments separated by a cation exchange membrane (Nafion N-117 membrane) with a continuously Ar or CO_2 gas injection. Each compartment contained 70 ml electrolyte (0.5 M $NaHCO_3$ made from de-ionized water). In a typical experiment, a standard three electrode setup in 0.5 M $NaHCO_3$ solution was assembled: an Ag/AgCl electrode as reference electrode, a Pt wire as auxiliary electrode and a carbon paper coated with the different samples as working electrode (surface area = 1 cm^2). The potentials were measured versus Ag/AgCl and converted to the reversible hydrogen electrode (RHE) according to the following equation: $E_{RHE} = E^0_{Ag/AgCl} + E_{Ag/AgCl} + 0.059 \times pH$, pH=7.[6] All electrochemical results were showed without iR-compensation by using a computer-controlled BioLogic VMP3 electrochemical workstation. Meanwhile, the linear sweep voltammetry (LSV) was performed to reach a stable state at a scan rate of 20 mV/s from 0 V to −1.0 V vs. RHE in Ar-saturated 0.5 M $NaHCO_3$ (pH=8.5) and CO_2-

saturated 0.5 M $NaHCO_3$ (pH=7) as supporting electrolyte. The cyclic voltammetry (CV) curves were performed at a scan rate of 20 mV/s.

Before the electrochemical CO_2 reduction experiments, an average rate of 20 mL/min Ar was injected into the cathodic electrolyte in order to form an Ar-saturated solution. During electrochemical CO_2 reduction experiments, the CO_2 gas was delivered at an average rate of 20 mL/min at room temperature and ambient pressure, measured downstream by a volumetric digital flowmeter. The gas phase composition was analyzed by gas chromatography (GC) during potentiostatic measurements every 20 min. The calibration of peak area vs. gas concentration was used for the molar quantification of each gaseous effluent. The Faradaic efficiency was calculated by determining the number of coulombs needed for each product and then dividing by the total charge passed during the time of the GC sampling according to the flow rate. Liquid products were analyzed afterwards by quantitative ^{1}H-NMR using water as the deuterated solvent.

Calculation Method:

Details concerning the calculation of mass activity and Faradaic Efficiency (FE) are shown as below.[6-8]

The mass activity (A/g) is calculated from the mass loading density (m) of catalyst (1.0 mg cm^{-2}) and the measured partial current density j (mA/cm^2) at −0.50 V vs. RHE.

mass activity $=j_{CO}/m$

The partial current density for a given gas product was calculated as below:

$$j_i = x_i \times V \times \frac{n_i F P_0}{RT} \times (electrode\ area)^{-1}$$

Where x_i is the volume fraction of certain product determined by online GC referenced to calibration curves from three standard gas samples, v is the flow rate, n_i is the number of electrons involved, P_0= 101.3 kPa, F is the Faraday constant, and R is the gas constant. The corresponding FE at each potential is calculated by

$$FE = \frac{j_i}{j} \times 100\ \%$$

DFT Calculations:

The spin-polarized DFT calculations with projector augmented wave (PAW) method [9-12] were performed using the Vienna Ab initio Simulation Package (VASP) code.[13] The Bayesian error estimation functional with van der Waals correlation (BEEF-vdW) was employed to set the plane wave basis.[14] The convergence criteria was 0.05 eV/ Å in force and 1×10^{-4} eV in energy and the plane wave cutoff was 500 eV. The Monkhorst–Pack mesh k-point grids was 2×2×1 for all models. All the vacuum thicknesses were higher than 15 Å. With the BEEF-vdW function, the energy of the gas phase molecules gave a systematic correction by +0.41 and +0.09 eV for gaseous CO_2 and H_2, respectively.[15-17] For the electroreduction of CO_2 to CO, the following elementary steps were considered:

$$CO_2(g) + * + H^+(aq) + e^- \leftrightarrow COOH* \quad \text{(Equation S.1)}$$

$$COOH* + H^+(aq) + e^- \leftrightarrow CO* + H_2O(l) \quad \text{(Equation S.2)}$$

$$CO* \leftrightarrow CO(g) + * \quad \text{(Equation S.3)}$$

where (g), (aq) represent the gaseous phase and aqueous phase, respectively. The *, COOH* and CO* represent free site, adsorption state of COOH and CO, respectively. The reaction free energies of each steps were calculated by following formula:

$$G = E_{\mathrm{DFT}} + E_{\mathrm{ZPE}} + \int C_p \mathrm{d}T - TS + E_{\mathrm{sol}} \quad \text{(Equation S.4)}$$

Where E_{DFT} is the DFT calculated energy, E_{ZPE} is the zero-point energy, C_p is the constant pressure heat capacity, T is temperture, S is the entropy and E_{sol} is solvation

correction and for CO* was stabilized by 0.1 eV and COOH* by 0.25 eV.[18] The temperature of the reaction is 298.15 K. The free energy corrections for each species are shown in **Table S3**.[19]

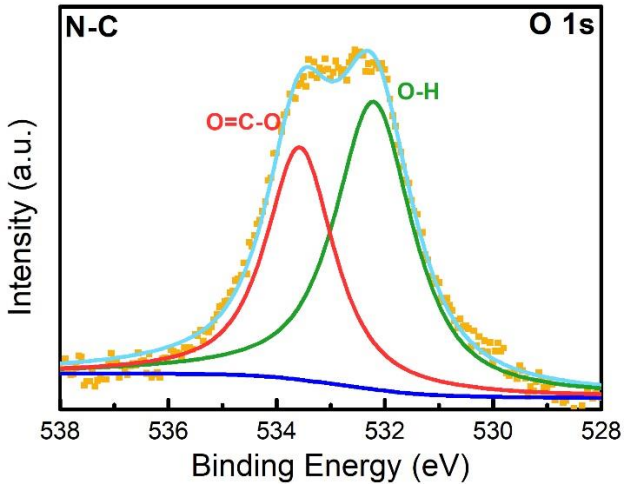

Figure S1. High-resolution XPS O 1s spectrum of N-C sample.

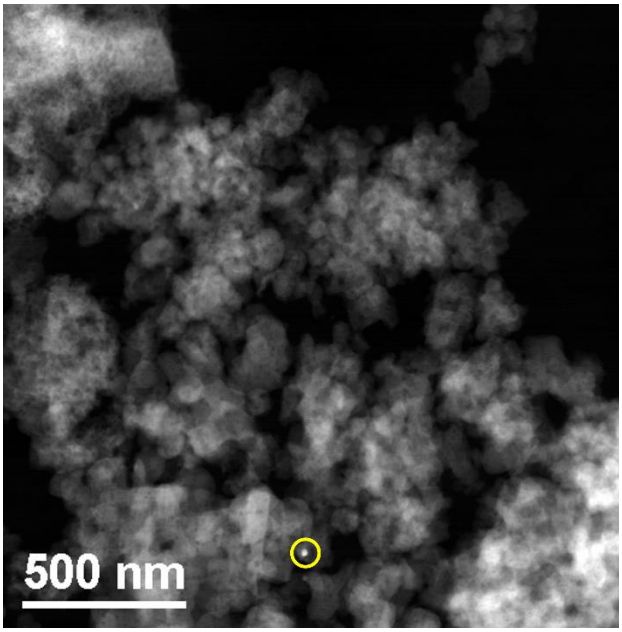

Figure S2. HAADF-STEM image of O-Fe-N-C. The yellow circle is highlighting the presence of only one Fe cluster in the large area examined.

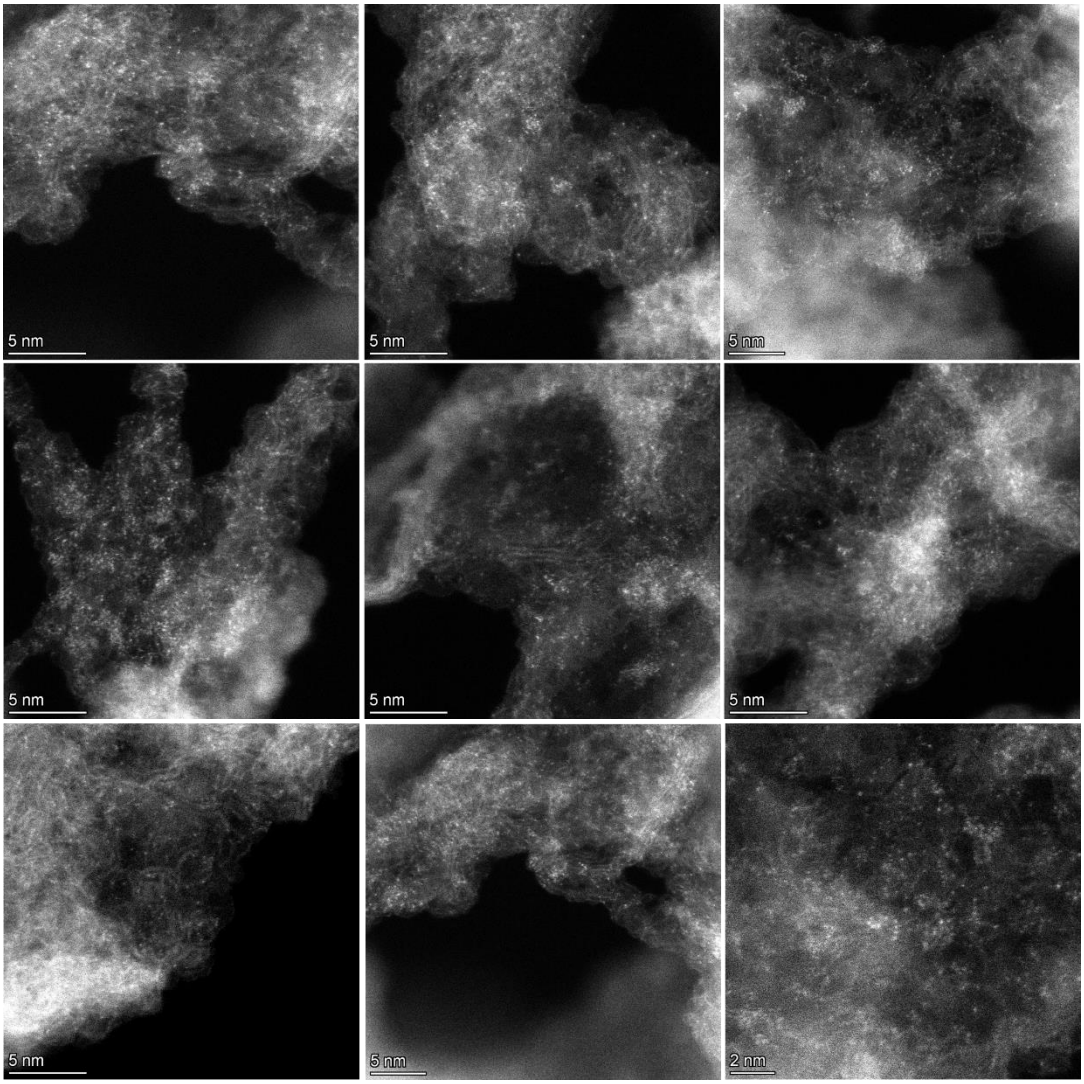

Figure S3. HAADF-STEM images of the O-Fe-N-C sample.

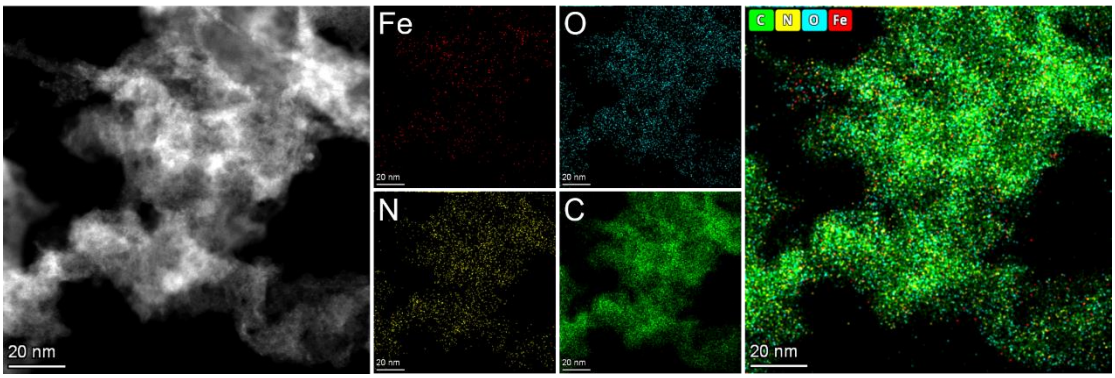

Figure S4. HAADF-STEM image of O-Fe-N-C and representative EDS chemical composition maps obtained from the corresponding STEM micrograph.

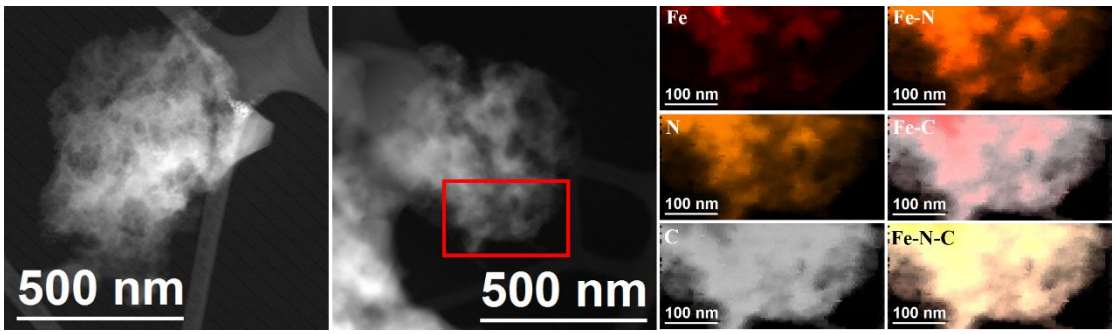

Figure S5. HAADF-STEM image of Fe-N-C and representative EELS chemical composition maps obtained from the red squared area of the STEM micrograph. Individual Fe $L_{2,3}$-edges at 708 eV (red), N K-edges at 401 eV (orange) and C K-edges at 285 eV (grey) as well as composites of Fe-N and Fe-C.

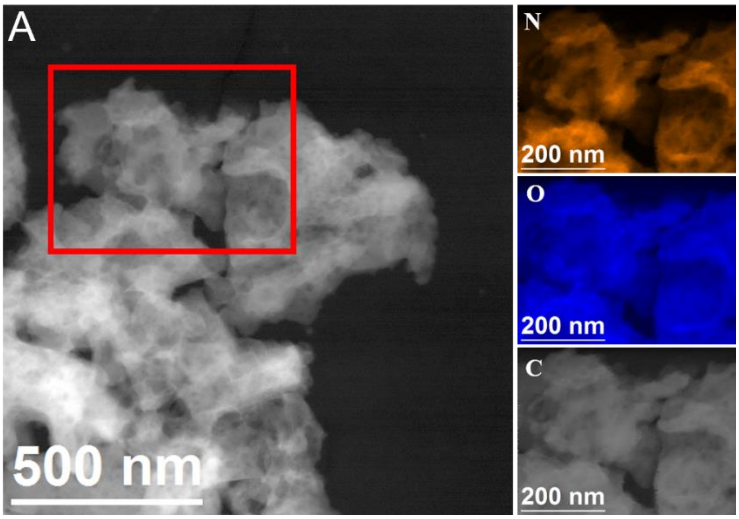

Figure S6. HAADF-STEM image of N-C and representative EELS chemical composition maps obtained from the red squared area of the STEM micrograph. Individual N K-edges at 401 eV (orange), O K-edges at 532 eV (blue) and C K-edges at 285 eV (grey).

Table S1. EXAFS fitting parameters at the Fe K-edge for various samples

Sample	Shell	N [a]	R (Å) [b]	σ^2 (Å^2·10^{-3}) [c]	ΔE0 (eV) [d]	*R* factor (%)
O-Fe-N-C	Fe-N(O)	5.1	2.02	9.8	0.2	0.8
	Fe-Fe	0.4	2.54	4.9	0.6	

[a] *N*: coordination numbers; [b] *R*: bond distance; [c] σ^2: Debye-Waller factors; [d] ΔE_0: the inner potential correction. *R* factor: goodness of fit. *S*02 were set as 0.85/0.90 for Fe-N/Fe-Fe, which were obtained from the experimental EXAFS fit of reference FePc/Fefoil by fixing CN as the known crystallographic value and was fixed to all the samples.

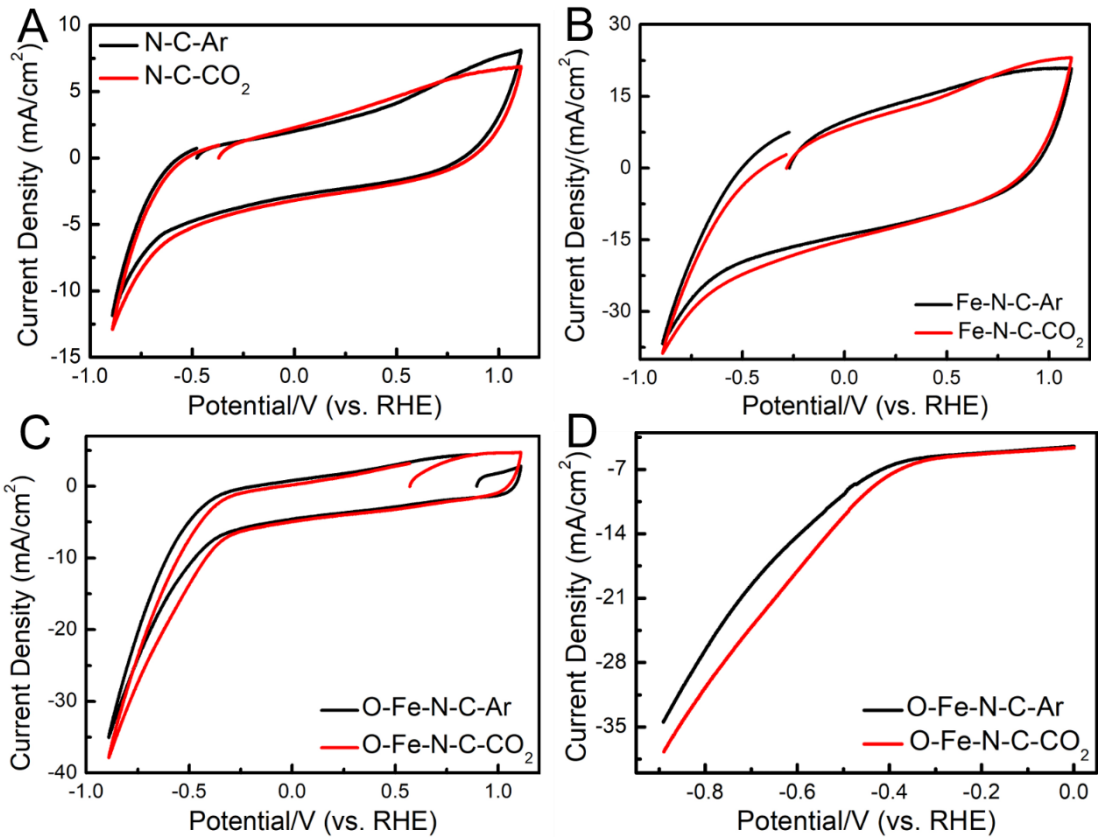

Figure S7. Cyclic voltammograms curves vs. RHE of (A) N-C, (B) Fe-N-C and (C) O-Fe-N-C obtained in Ar or CO_2-saturated 0.5 M $NaHCO_3$ solution. (D) is the LSV comparison for O-Fe-N-C in Ar-and CO_2-saturated 0.5 M $NaHCO_3$ solution.

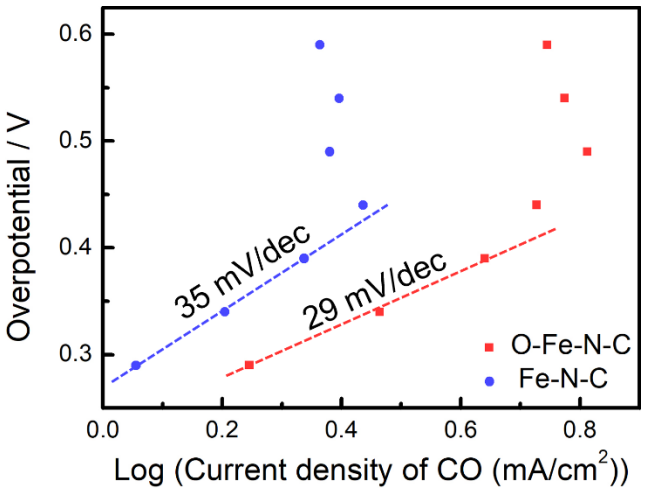

Figure S8. Tafel slope of O-Fe-N-C and Fe-N-C samples.

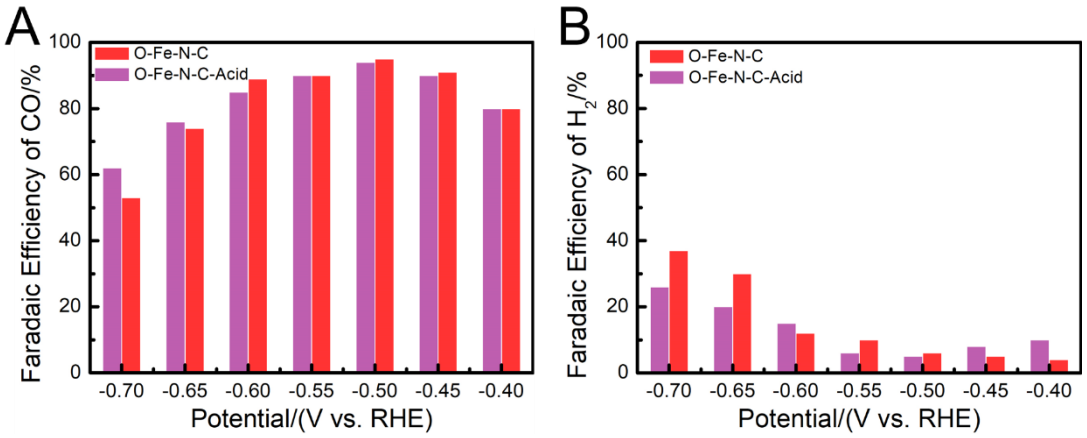

Figure S9. (A) FE of CO at various potentials and (B) FE of H_2 at various potentials on O-Fe-N-C and O-Fe-N-C-Acid.

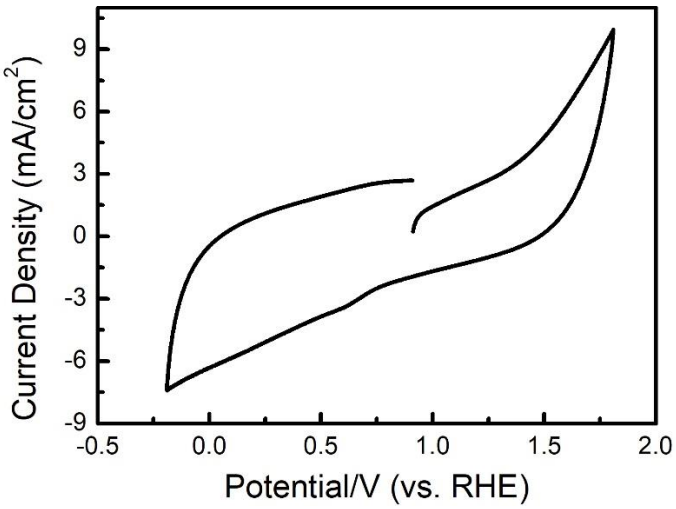

Figure S10. CV curves of O-Fe-N-C in 0.5 M Ar-saturated $NaHCO_3$ electrolyte.

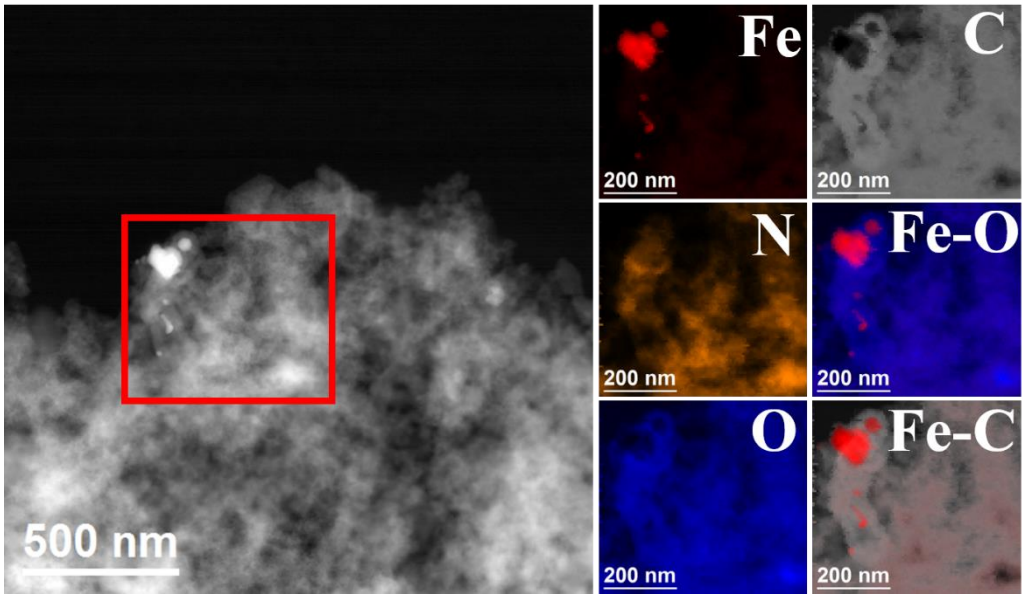

Figure S11. HAADF-STEM image of O-Fe-N-C and representative EELS chemical composition maps obtained from the red squared area of the STEM micrograph. Individual Fe $L_{2,3}$-edges at 708 eV (red), N K-edges at 401 eV (orange), O K-edges at 532 eV (blue) and C K-edges at 285 eV (grey) as well as composites of Fe-O and Fe-C.

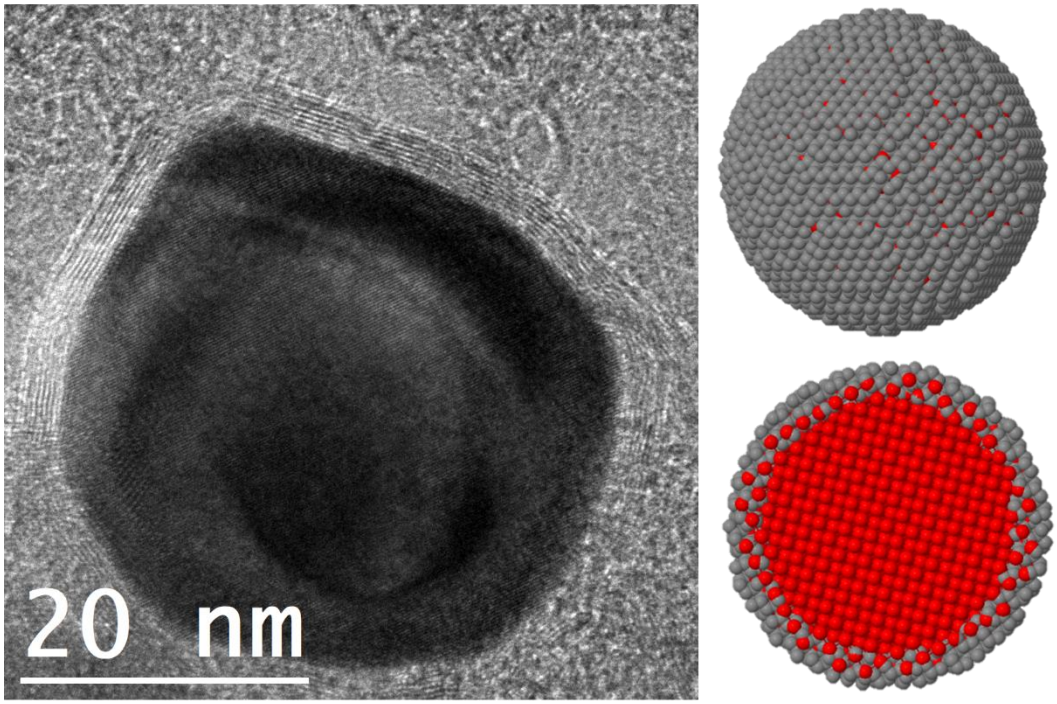

Figure S12. HRTEM micrographs of O-Fe-N-C sample as well as atomic supercell model illustration of the Fe nanoparticle with carbon shell (Fe and C are represented in red and grey, respectively).

Table S2. Fe loading ratios of different samples.

Samples	Feeding mass (Fe)	Acid treatment	Final product ratio (Fe)
O-Fe-N-C	20 μL	No	0.73 %
O-Fe-N-C	20 μL	Yes	0.41 %

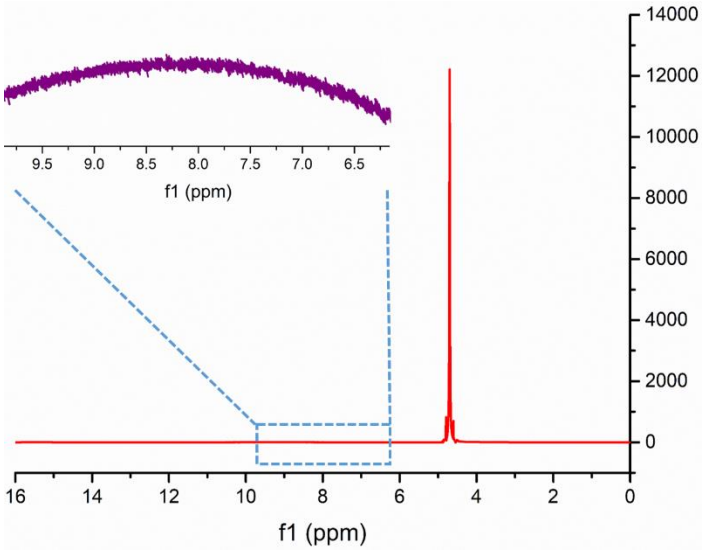

Figure S13. The representative ^{1}H-NMR spectra of the electrolyte after electrolysis of −0.50 V for O-Fe-N-C in CO_2-saturated 0.5 M $NaHCO_3$ electrolyte for 30 h.

Table S3. Parameters used for the free energy corrections. T = 298.15 K.

Species	ZPE (eV)	$\int C_p \, dT$ (eV)	$-TS$ (eV)
H_2	0.28	0.09	-0.40
CO_2	0.31	0.11	-0.66
CO	0.13	0.09	-0.61
H_2O	0.58	0.10	-0.67
H*	0.19	0.01	-0.01
CO*	0.22	0.08	-0.16
COOH*	0.62	0.10	-0.19

Table S4. Faradaic Efficiency (CO) of the reported single atom electrocatalysts for CO_2 electroreduction.

Catalyst	Product	FE(CO)	Potential	Reference
Fe^{3+}@NG	CO	85 %	−0.68 V vs. RHE	[20]
Fe-N-C	CO	81 %	−0.57 V vs. RHE	[21]
Fe-N-C	CO	80 %	−0.50 V vs. RHE	[22]
Fe-N-PC	CO	90 %	−0.49 V vs. RHE	[23]
Fe^{3+}-N-C	CO	90 %	−0.47 V vs. RHE	[24]
NPPCN	CO	95.9 %	−0.70 V vs. RHE	[25]
Fe-N-C	CO	95 %	−0.64 V vs. RHE	[26]
Fe/NCS	CO	87 %	−0.45 V vs. RHE	[27]
Fe-N-C	CO	93 %	−0.58 V vs. RHE	[28]
Fe-N-C	CO	86.9 %	−0.47 V vs. RHE	[29]
Bi SAC/NC	CO	97 %	−0.50 V vs. RHE	[30]
Ni-N-C	CO	71.9 %	−0.90 V vs. RHE	[8]
Ni-N-C	CO	98 %	−0.80 V vs. RHE	[31]
Ni-N-C	CO	98 %	−1.03 V vs. RHE	[32]
Co-N-C	CO	94 %	−0.775 V vs. RHE	[33]
Co-N_5/HNPCs	CO	99.4 %	−0.80 V vs. RHE	[34]
Co-N-C	CO	91 %	−0.60 V vs. RHE	[35]
Ni-N-C	CO	96 %	−0.70 V vs. RHE	[36]
Ni-N-C	CO	95 %	−0.90 V vs. RHE	[37]
Ag SAC/MnO_2	CO	95.7 %	−0.85 V vs. RHE	[38]
Ni-N-C	CO	96 %	−0.80 V vs. RHE	[39]
Ni-N-C	CO	95.6 %	−0.65 V vs. RHE	[40]
Pd-N_4	CO	55 %	−0.50 V vs. RHE	[41]
Ni-N_4/C-NH_2	CO	95 %	−0.70 V vs. RHE	[42]
FeN_5-C	CO	~97 %	−0.46 V vs. RHE	[43]
Ni-N-C	CO	97 %	−0.80 V vs. RHE	[44]
Ni-N-C	CO	~97 %	−0.66 V vs. RHE	[45]
Ni-N-C	CO	96 %	−0.86 V vs. RHE	[46]
Cu-N-C	CO	96 %	−0.70 V vs. RHE	[47]
Ni-N-C	CO	~100 %	−0.75 V vs. RHE	[7]
O-Fe-N-C	**CO**	**95 %**	**−0.50 V vs. RHE**	**This work**

References

[1] B. Ravel, M. Newville, *J. Synchrotron Rad.,* **2005,** *12*, 537-541.

[2] H. Baumgartel, *Technik und Laboratorium*, **1988,** *36*, 650-650.

[3] J.J. Rehr, R.C. *Rev. Modern Phys.*, **2000,** *72*, 621-654.

[4] S.J. Lyle, R.W. Flaig, K.E. Cordova, O.M. Yaghi, *J. Chem. Education*, **2018,** *95*, 1512-1519.

[5] S. Dou, J. Song, S. Xi, Y. Du, J. Wang, Z.-F. Huang, Z.J. Xu, X. Wang, *Angew. Chem. Int. Ed.*, **2019,** *58*, 4041-4045.

[6] T. Zhang, J. Du, P. Xi, C. Xu, *ACS Appl. Mater. Interfaces*, **2017,** *9*, 362-370.

[7] T. Zheng, K. Jiang, N. Ta, Y. Hu, J. Zeng, J. Liu, H. Wang, *Joule*, **2019,** *3*, 265-278.

[8] C. Zhao, X. Dai, T. Yao, W. Chen, X. Wang, J. Wang, J. Yang, S. Wei, Y. Wu, Y. Li, *J. Am. Chem. Soc.*, **2017,** *139*, 8078-8081.

[9] P.E. Blöchl, *Phys. Rev. B*, **1994,** *50*, 17953-17979.

[10] G. Kresse, J. Furthmüller, *Phys. Rev. B*, **1996,** *54*, 11169-11186.

[11] G. Kresse, J. Furthmüller, *Comput. Mater. Sci.*, **1996,** *6*, 15-50.

[12] G. Kresse, D. Joubert, *Phys. Rev. B*, **1999,** *59*, 1758-1775.

[13] J. Hafner, *J. Comput. Chem.*, **2008,** *29*, 2044.

[14] J. Wellendorff, K.T. Lundgaard, A. Møgelhøj, V. Petzold, D.D. Landis, J.K. Nørskov, T. Bligaard, K.W. Jacobsen, *Phys. Rev. B*, **2012,** *85*, 235149.

[15] F. Studt, M. Behrens, E.L. Kunkes, N. Thomas, S. Zander, A. Tarasov, J. Schumann, E. Frei, J.B. Varley, F. Abild-Pedersen, J.K. Nørskov, R. Schlögl, *ChemCatChem*, **2015,** *7*,1105-1111.

[16] F. Studt, F. Abild-Pedersen, J.B. Varley, J.K. Nørskov, *Catal. Lett.*, **2013,** *143*, 71-73.

[17] R. Christensen, H.A. Hansen, T. Vegge, *Catal. Sci. Technol.*, **2015,** *5*, 4946-4949.

[18] A.A. Peterson, F. Abild-Pedersen, F. Studt, J. Rossmeisl, J.K. Norskov, *Energy Environ. Sci.*, **2010,** *3*, 1311-1315.

[19] K. Chan, C. Tsai, H.A. Hansen, J.K. Nørskov, *ChemCatChem*, **2014,** *6*, 1899-1905.

[20] W. Bi, X. Li, R. You, M. Chen, R. Yuan, W. Huang, X. Wu, W. Chu, C. Wu, Y. Xie, *Adv. Mater.*, **2018,** *30*, 1706617.

[21] X.-M. Hu, H.H. Hval, E.T. Bjerglund, K.J. Dalgaard, M.R. Madsen, M.-M. Pohl, E. Welter, P. Lamagni, K.B. Buhl, M. Bremholm, M. Beller, S.U. Pedersen, T. Skrydstrup, K. Daasbjerg, *ACS Catal.*, **2018,** *8*, 6255-6264.

[22] T.N. Huan, N. Ranjbar, G. Rousse, M. Sougrati, A. Zitolo, V. Mougel, F. Jaouen, M. Fontecave, *ACS Catal.*, **2017,** *7*, 1520-1525.

[23] Y. Chen, L. Zou, H. Liu, C. Chen, Q. Wang, M. Gu, B. Yang, Z. Zou, J. Fang, H. Yang, *J. Phys. Chem. C*, **2019,** *123*, 16651-16659.

[24] J. Gu, C.-S. Hsu, L. Bai, H.M. Chen, X. Hu, *Science*, **2019,** *364*, 1091-1094.

[25] J. Tuo, Y. Zhu, L. Cheng, Y. Li, X. Yang, J. Shen, C. Li, *ChemSusChem*, **2019,** *12*, 2644-2650.

[26] S. Wu, X. Lv, D. Ping, G. Zhang, S. Wang, H. Wang, X. Yang, D. Guo, S. Fang, *Electrochim. Acta*, **2020,** *340*, 135930.

[27] Y. Zhu, X. Li, X. Wang, K. Lv, G. Xiao, J. Feng, X. Jiang, M. Fang, Y. Zhu, *ChemistrySelect*, **2020,** *5*, 1282-1287.

[28] F. Pan, H. Zhang, K. Liu, D. Cullen, K. More, M. Wang, Z. Feng, G. Wang, G. Wu, Y. Li, *ACS Catal.*, **2018,** *8*, 3116-3122.

[29] X. Chen, D.-D. Ma, B. Chen, K. Zhang, R. Zou, X.-T. Wu, Q.-L. Zhu, *Appl. Catal. B: Environ.*, **2020,** *267*, 118720.

[30] E. Zhang, T. Wang, K. Yu, J. Liu, W. Chen, A. Li, H. Rong, R. Lin, S. Ji, X. Zheng, Y. Wang, L. Zheng, C. Chen, D. Wang, J. Zhang, Y. Li, *J. Am. Chem. Soc.*, **2019,** *141*, 16569-16573.

[31] Y.-N. Gong, L. Jiao, Y. Qian, C.-Y. Pan, L. Zheng, X. Cai, B. Liu, S.-H. Yu, H.-L. Jiang, *Angew. Chem. Int. Ed.*, **2020,** *59*, 2705-2709.

[32] C. Yan, H. Li, Y. Ye, H. Wu, F. Cai, R. Si, J. Xiao, S. Miao, S. Xie, F. Yang, Y. Li, G. Wang, X. Bao, *Energy Environ. Sci.*, **2018,** *11*, 1204-1210.

[33] X. Wang, Z. Chen, X. Zhao, T. Yao, W. Chen, R. You, C. Zhao, G. Wu, J. Wang, W. Huang, J. Yang, X. Hong, S. Wei, Y. Wu, Y. Li, *Angew. Chem. Int. Ed.*, **2018,** *57*, 1944-1948.

[34] Y. Pan, R. Lin, Y. Chen, S. Liu, W. Zhu, X. Cao, W. Chen, K. Wu, W.-C. Cheong, Y. Wang, L. Zheng, J. Luo, Y. Lin, Y. Liu, C. Liu, J. Li, Q. Lu, X. Chen, D. Wang, Q. Peng, C. Chen, Y. Li, *J. Am. Chem. Soc.*, **2018,** *140*, 4218-4221.

[35] H. Yang, Q. Lin, Y. Wu, G. Li, Q. Hu, X. Chai, X. Ren, Q. Zhang, J. Liu, C. He, *Nano Energy*, **2020,** 70, 104454.

[36] H. Yang, Q. Lin, C. Zhang, X. Yu, Z. Cheng, G. Li, Q. Hu, X. Ren, Q. Zhang, J. Liu, C. He, *Nature Commun.*, **2020,** *11*, 593.

[37] W. Xiong, H. Li, H. Wang, J. Yi, H. You, S. Zhang, Y. Hou, M. Cao, T. Zhang, R. Cao, *Small*, **2020,** *16*, 2003943.

[38] N. Zhang, X. Zhang, L. Tao, P. Jiang, C. Ye, R. Lin, Z. Huang, A. Li, D. Pang, H. Yan, Y. Wang, P. Xu, S. An, Q. Zhang, L. Liu, S. Du, X. Han, D. Wang, Y. Li, *Angew. Chem. Int. Ed.*, **2021,** *60*, 6170-6176.

[39] X. Rong, H.-J. Wang, X.-L. Lu, R. Si, T.-B. Lu, *Angew. Chem. Int. Ed.*, **2020,** *59*, 1961-1965.

[40] Y. Zhang, L. Jiao, W. Yang, C. Xie, H.-L. Jiang, *Angew. Chem. Int. Ed.*, **2021,** DOI: 10.1002/anie.202016219.

[41] Q. He, J.H. Lee, D. Liu, Y. Liu, Z. Lin, Z. Xie, S. Hwang, S. Kattel, L. Song, J.G. Chen, *Adv. Func. Mater.*, **2020,** *30*, 2000407.

[42] Z. Chen, X. Zhang, W. Liu, M. Jiao, K. Mou, X. Zhang, L. Liu, *Energy Environ. Sci.*, **2021**, DOI: 10.1039/D0EE04052E.

[43] H. Zhang, J. Li, S. Xi, Y. Du, X. Hai, J. Wang, H. Xu, G. Wu, J. Zhang, J. Lu, J. Wang, *Angew. Chem. Int. Ed.*, **2019,** *58*, 14871-14876.

[44] K. Jiang, S. Siahrostami, T. Zheng, Y. Hu, S. Hwang, E. Stavitski, Y. Peng, J. Dynes, M. Gangisetty, D. Su, K. Attenkofer, H. Wang, *Energy Environ. Sci.*, **2018,** *11*, 893-903.

[45] X. Wang, S. Ding, T. Yue, Y. Zhu, M. Fang, X. Li, G. Xiao, Y. Zhu, L. Dai, *Nano Energy*, **2021,** *82*, 105689.

[46] Y. Lu, H. Wang, P. Yu, Y. Yuan, R. Shahbazian-Yassar, Y. Sheng, S. Wu, W. Tu, G. Liu, M. Kraft, R. Xu, *Nano Energy*, **2020,** *77*, 105158.

[47] F. Yang, X. Mao, M. Ma, C. Jiang, P. Zhang, J. Wang, Q. Deng, Z. Zeng, S. Deng, *Carbon*, **2020,** *168*, 528-535.